

## Photolysis and the dimethylsulfide (DMS) summer paradox in the Sargasso Sea

*Dierdre A. Toole*

Institute for Computational Earth System Science; Interdepartmental Graduate Program in Marine Science,  
University of California–Santa Barbara, Santa Barbara, California 93106

*David J. Kieber*

State University of New York, College of Environmental Science and Forestry, Chemistry Department,  
Syracuse, New York 13210

*Ronald P. Kiene*

Department of Marine Sciences, University of South Alabama, Mobile, Alabama 36688

*David A. Siegel and Norman B. Nelson*

Institute for Computational Earth System Science, University of California–Santa Barbara,  
Santa Barbara, California 93106

### Abstract

Apparent quantum yields and rates of dimethylsulfide (DMS) photolysis were determined from Sargasso Sea seawater with the goal of assessing the extent to which photoreactions affect the unusually elevated upper ocean concentrations of DMS during the summer, the so-called DMS summer paradox. Apparent quantum yields determined with monochromatic radiation decrease exponentially with increasing wavelength and indicate that DMS photolysis is driven by ultraviolet (UV) radiation. The relative spectral partitioning differs between samples collected from the surface mixed layer (15 m) and from the chlorophyll *a* maximum (80 m), presumably because of differences in chromophoric dissolved organic matter (CDOM) quality (e.g., apparent degree of bleaching). Quantum yields are also temperature dependent, and an approximate doubling of photolysis rates occurs for a 20°C increase in temperature. The significance of DMS photolysis to upper ocean sulfur budgets is explored using a multiyear (1992–1994) DMS time series, concurrent irradiance determinations and temperature profiles, and estimates of CDOM absorption. Depth-integrated, mixed-layer DMS photolysis rates peak in the summer (15–25  $\mu\text{mol m}^{-2} \text{d}^{-1}$ ) and decline to  $<1 \mu\text{mol m}^{-2} \text{d}^{-1}$  in the winter. These rates correspond to specific turnover rates of  $\sim 0.29 \text{d}^{-1}$  in the summer and  $<0.02 \text{d}^{-1}$  in the winter. Seasonal changes in solar radiation, temperature, and DMS concentrations drive the 30-fold differences in photolysis rates, overshadowing differences caused by photosensitizer (CDOM) quantity or quality (21–35%). These results demonstrate that although photolysis is not the primary driver of the summer paradox, it makes an important contribution to the time–depth pattern of DMS concentrations observed in the Sargasso Sea.

The biogeochemical cycling of sulfur between the upper water column of the ocean and the atmospheric marine boundary layer has received a great deal of attention over the last several decades because of its implication in a cloud albedo feedback loop (e.g., Shaw 1983; Bates et al. 1987; Charlson et al. 1987). The biogenic production of dimethylsulfide (DMS) in the marine environment is an important source of atmospheric sulfur. Although DMS concentrations exhibit considerable spatial and temporal variability, DMS

is ubiquitous in the ocean, representing  $>90\%$  of the oceanic sulfur flux and  $>50\%$  of the global biogenic flux to the atmosphere (Andreae 1986). DMS is derived from the enzymatic cleavage of dimethylsulfoniopropionate (DMSP), which is synthesized in phytoplankton at species-dependent concentrations (Keller et al. 1989). Bulk water column DMS concentrations are a result of the balance between bacteria-, phytoplankton-, and zooplankton-mediated production mechanisms and loss mechanisms that primarily consist of sea–air flux, bacterial consumption, and photolysis (e.g., Dacey and Wakeham 1986; Kiene and Bates 1990; Kieber et al. 1996; Simó and Pedrós-Alió 1999b). Because of the complex coupled physical, biological, and chemical processes involved in the marine sulfur cycle, an assessment of the patterns of DMS variability requires a complete understanding of the substances and mechanisms associated with each pathway.

Photolysis is an important removal process for upper ocean DMS (e.g., Brimblecombe and Shooter 1986; Kieber et al. 1996; Brugger et al. 1998; Hatton 2002). Photolysis occurs through a secondary photosensitized pathway because

### Acknowledgments

This work was supported by NASA under an Earth System Science Fellowship and the SIMBIOS Program. We are extremely grateful to John Dacey for the use of his DMS and DMSP time series datasets. The authors acknowledge George Westby and Todd Medovich (SUNY-ESF) for their assistance with laboratory photolysis studies; Rod Johnson, Paul Lethaby, Rachel Parsons, Chrissy Van Hilst, Karen Paterson, and the many BATS technicians for their assistance at sea; and Andrew Hall, Toby Westberry and two anonymous reviewers for their assistance with the development of this manuscript.

DMS does not absorb light at wavelengths  $>260$  nm (Brimblecombe and Shooter 1986). The exact composition and activity of the chromophoric photosensitizers remains unclear, however, and total absorption by chromophoric dissolved organic matter (CDOM) can be used as a proxy (Kieber et al. unpubl.). Hence, photolysis can be modeled as a function of an apparent quantum yield and the photon flux absorbed by CDOM. From the northern Adriatic Sea, Brügger et al. (1998) showed that DMS photolysis was proportional to the irradiance intensity and dissolved organic carbon (DOC) concentrations. DOC and CDOM concentrations are not related in the open ocean, however (Siegel and Michaels 1996; Nelson et al. 1998; Siegel et al. 2002). It is critical to make this distinction because the colored and non-colored components of the dissolved organic matter pool have distinct, independent, annual cycles (Nelson and Siegel 2002). Accurate photolysis parameterizations will greatly enhance current DMS models and, as a result, our understanding of DMS cycling. At present, photolysis rates are poorly constrained, assumed constant in space and time, or simply omitted (e.g., Van den Berg et al. 1996; Simó and Pedró-Alió 1999b; Jodwalis et al. 2000).

The multiyear Dacey et al. (1998) DMS time series collected as part of the U.S. Joint Global Ocean Flux Study (JGOFS) Bermuda Atlantic Time-series Study (BATS) demonstrates the so-called summer paradox (Simó and Pedró-Alió 1999a). The essence of the paradox is that DMS concentrations reach their maximum throughout the water column in July and August, more than 2 months later than the maximum for its precursor, DMSP (Fig. 1A,B). The timing of the DMS maximum is additionally puzzling because it coincides with the seasonal minimum in phytoplankton pigment biomass and primary production. Summer mean mixed-layer chlorophyll concentrations are  $\sim 0.05$   $\text{mg m}^{-3}$ , indicating extremely oligotrophic conditions (Fig. 1C). Mean mixed-layer DMS concentrations also have an inverse relationship with CDOM absorption (Fig. 1E). This relationship led Siegel and Michaels (1996) to hypothesize that the summertime buildup of DMS results from reduced photolysis rates. Although incident ultraviolet (UV, 280–400 nm) and photosynthetically available radiation (PAR, 400–700 nm) fluxes are larger in the summer (Fig. 1D), the concurrent, extremely low CDOM concentrations (Fig. 1E) suggest lower absorbed quanta, and thereby photolysis rates, in the upper meter (Siegel and Michaels 1996). Knowledge of the functional dependences of the apparent quantum yield is required to properly assess how the photon flux absorbed by CDOM translates to the photochemical destruction of DMS in the photic zone.

Here, we determine wavelength and temperature-dependent apparent quantum yields for DMS photolysis in the Sargasso Sea. Broadband solar and monochromatic incubation experiments are conducted to determine the spectral regions primarily responsible for DMS photolysis in this open ocean region. The seasonal importance of DMS photolysis is explored using the Dacey et al. (1998) DMS dataset and the extensive time series datasets collected in conjunction with the BATS and Hydrostation S sampling programs, allowing the controlling factors to be elucidated. A primary goal in

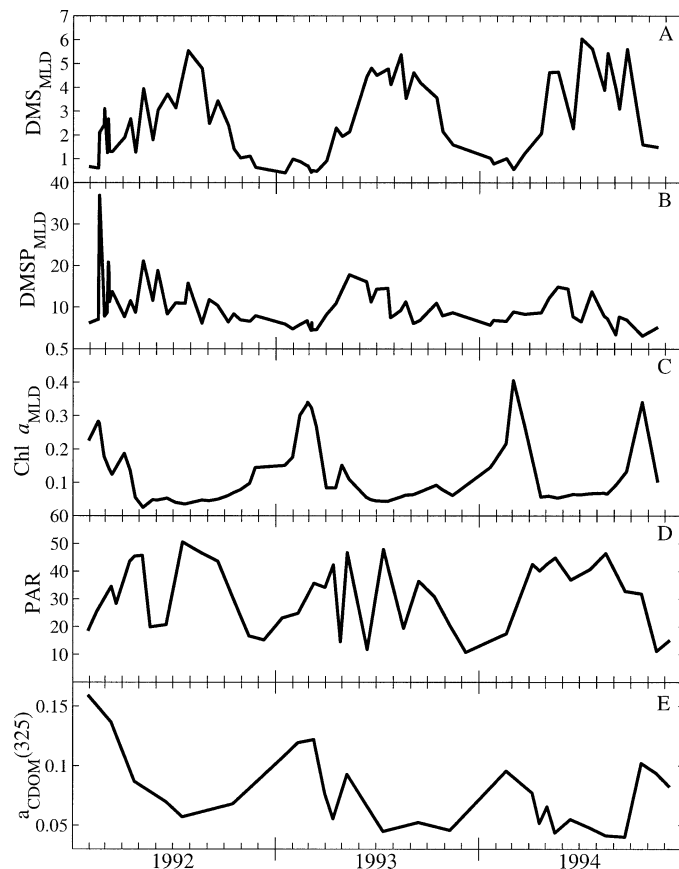


Fig. 1. Time series of (A) mean mixed-layer DMS concentrations ( $\text{nmol L}^{-1}$ ), (B) mean mixed-layer total (dissolved + particulate) DMSP concentrations ( $\text{nmol L}^{-1}$ ), (C) mean mixed-layer Chl *a* concentrations ( $\text{mg m}^{-3}$ ), (D) daily integrated surface photosynthetically available radiation (PAR) ( $\text{mol quanta m}^{-2} \text{d}^{-1}$ ), and (E) modeled chromophoric dissolved organic matter absorption coefficient at 325 nm ( $\text{m}^{-1}$ ).  $a_{\text{CDOM}}(325)$  was modeled using the globally optimized semianalytical UCSB IOP inversion model (Maritorena et al. 2002) and extended into the UV using the functional relationship described in Eq. 1. DMS and DMSP 1992–1993 data are from Dacey et al. (1998). Data are shown from January 1992 through November 1994.

this analysis is to quantify the role that photolysis plays in driving the observed summer paradox in the Sargasso Sea.

## Materials and methods

**Shipboard sampling**—The northern Sargasso Sea has a well-documented seasonal cycle characterized as seasonally oligotrophic with a variable-strength spring bloom. The onset of warming in the spring leads to a well-stratified water column with a shallow mixed layer in the summer that progressively deepens via convective overturn to mixed-layer depths in excess of 100 m in the winter (Steinberg et al. 2001). Water samples were collected from the BATS site (water depth  $\sim 4,680$  m), nominally located 85 km southeast of the island of Bermuda. Samples were collected from the surface mixed layer (15 m) and the chlorophyll *a* (Chl *a*) maximum (80 m) at 1030 h local time during a U.S. BATS

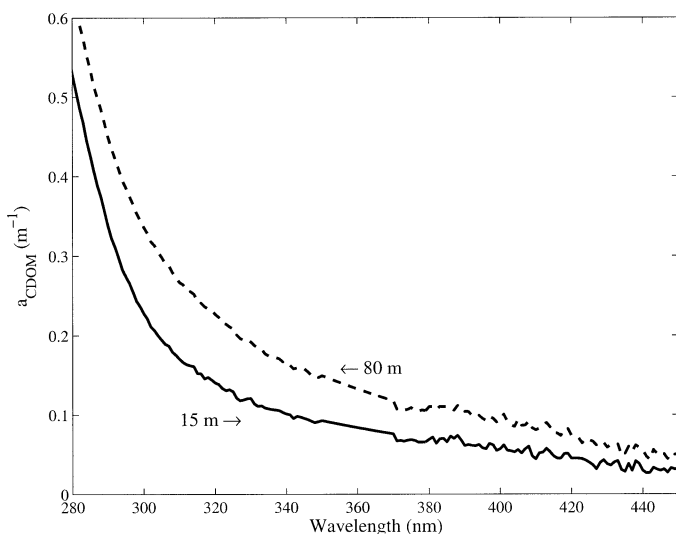


Fig. 2. CDOM absorption coefficient spectra for the 15- and 80-m samples ( $\text{m}^{-1}$ ). Data collected from the diode array were used for wavelengths 280–450 nm, with the exception of 350–370 nm, which were smoothed using the functional relationship described in Eq. 1.

core cruise (BATS 154) on 19 July 2001 aboard the R/V *Weatherbird II*. At this time of the year, because of seasonal stratification, surface waters are characterized by severely photobleached CDOM (Nelson et al. 1998). Reflecting this, the surface, 15-, and 25-m samples all had CDOM absorption coefficients  $<0.225 \text{ m}^{-1}$  at a wavelength of 300 nm. We chose to study the 80-m sample because its absorption coefficient was significantly higher ( $>0.300 \text{ m}^{-1}$ , Fig. 2). This depth region (60–85 m) is characterized by a seasonal maximum in UV light absorption because of local production of CDOM (Nelson et al. 1998).

Seawater samples were gravity filtered directly from Niskin bottles secured to the conductivity, temperature, and depth (CTD) rosette system. The samples were filtered using a Whatman POLYCAP 75 AS 0.2- $\mu\text{m}$  filter capsule (nylon membrane with a glass microfiber prefilter enclosed in a polypropylene housing) attached to the Niskin bottles with silicon tubing. Prior to sample collection, filter capsules were rinsed with Milli-Q water and acetonitrile (Burdick and Jackson, distilled in glass grade) until the fluorescence at 400 nm was zero as determined by flow-injection analysis (Miller 2000). Unless otherwise noted, all glassware used in this study, including the Qorpak bottles and their Teflon-lined caps, was cleaned by three rinses of Milli-Q water followed by three rinses each of 10% hydrofluoric acid, 10% hydrochloric acid, and 10% methanol (all chemicals were reagent grade or better). As a final step, the glassware was copiously rinsed with Milli-Q water to remove any chemical residue. The cleaned bottles were then baked in a muffle furnace at 350°C for at least 6 h and subsequently stored with a small amount of 10% hydrochloric acid prior to sampling. All glassware was rinsed copiously with the 0.2- $\mu\text{m}$ -filtered seawater sample at least five times before shipboard sample collection. The filtered seawater samples were stored at 4°C

in the pretreated 4-liter Qorpak bottles wrapped in aluminum foil to eliminate light exposure. In addition, all samples were drawn wearing powder-free polyethylene gloves to further avoid contamination. All refrigerated samples were transported back to the laboratory in Syracuse, New York, within 4 d of sampling and were reaerated prior to analysis with ultrahigh-purity air passed through high-capacity molecular sieve, drierite, and activated carbon cartridges.

**Chemicals and standards**—The DMS used for photochemical experiments was purchased from Aldrich, and DMS standards were made from DMSP hydrochloride purchased from Research Plus. Reagent-grade sodium hydroxide purchased from Fisher was used to convert DMSP hydrochloride into DMS. For details regarding calibrations and DMS additions to seawater for the photochemical experiments, the reader is referred to Kieber et al. (1996).

Calibrated DMS standards ( $\sim 2 \mu\text{mol L}^{-1}$  in Milli-Q water) were added to 0.2- $\mu\text{m}$ -filtered seawater to yield DMS concentrations ranging from 15 to 20  $\text{nmol L}^{-1}$ . DMS photolysis in seawater follows pseudo first-order kinetics at concentrations up to  $\sim 50\text{--}100 \text{ nmol L}^{-1}$ , above which it may approach zero-order kinetics (Kieber et al. 1996). Care was taken to stay well within the first-order concentration range.

**Laboratory analysis**—DMS concentrations were determined using a modified purge and trap method following Kiene and Service (1991). Briefly, 1 ml of sample was sparged for 2 min for analysis on a Shimadzu GC-14A gas chromatograph (GC) equipped with a flame photometric detector and a Chromosil 330 column (Supelco). The GC was operated at a column temperature of 60°C and a detector temperature of 225°C. All samples were analyzed in duplicate with analytical precision on the order of  $\pm 2\%$  at the 15  $\text{nmol L}^{-1}$  range.

CDOM absorption values were determined using a Hewlett Packard 8453 UV-visible (UV-VIS) photodiode array spectrophotometer equipped with a 5-cm quartz microliter flow cell, with Milli-Q water as the reference. To assess changes associated with sample transport, CDOM absorption values determined in Syracuse were compared to absorption spectra obtained with freshly collected samples in Bermuda using a Perkin Elmer Lambda 18 spectrophotometer equipped with matched 10-cm quartz cuvettes (Nelson et al. 1998). No statistically significant changes in CDOM absorption coefficients were observed relative to the initial absorption ( $<5\%$  differences were noted for the entire absorption spectrum). Absorption curves were corrected for offsets (assumed zero between 675 and 700 nm) and fit using a standard CDOM exponential functional relationship outlined in Green and Blough (1994).

$$a_{\text{CDOM}}(\lambda) = a_{\text{CDOM}}(\lambda_0)e^{-S(\lambda-\lambda_0)} \quad (1)$$

$\lambda$  is the wavelength,  $\lambda_0$  is the reference wavelength (320 nm),  $a_{\text{CDOM}}(\lambda)$  is absorption by CDOM at wavelength  $\lambda$ ,  $a_{\text{CDOM}}(\lambda_0)$  is CDOM absorption at 320 nm, and  $S$  is the exponential slope parameter derived from the slope of the natural log-transformed data versus wavelength from 290 to 350 nm.

*Monochromatic incubations*—Wavelength-dependent and temperature-dependent apparent quantum yields for DMS photolysis were determined according to the procedure outlined in Kieber et al. (1996). Briefly, apparent quantum yields were determined employing monochromatic irradiations with a 1,000-W xenon arc lamp and a Spectral Energy GM 252 high-intensity grating monochromator. All irradiations were carried out in a 1-cm quartz cell sealed with a Teflon-lined plastic cap with no headspace and containing a Teflon-covered stir bar. For each irradiation, the quartz cuvette was rinsed three times and was then allowed to overflow equivalent to two or three cell volumes to rinse out the previous sample. In the sample holder, the cell temperature was controlled by a Fisher 9008 recirculating ethylene glycol water bath. With the exception of the temperature study, all incubations were carried out at 21°C, and samples were allowed to equilibrate in the cell holder for 5 min prior to irradiation. The length of the irradiation varied from 20 to 960 min depending on wavelength and sample absorption. The bandwidth was set to 9.9 nm for wavelengths <360 nm and was increased to 19.5 nm for wavelengths ≥360 nm. In addition, for wavelengths >320 nm, a long-pass filter ( $\lambda < \sim 300$  nm were blocked) was placed between the monochromator and the sample to eliminate second-order diffraction. The irradiation wavelength and bandwidth were periodically verified employing a calibrated, Optronic OL 754 scanning spectroradiometer.

At the conclusion of an irradiation, the Teflon stopper was pierced twice with PEEK tubing. One tube was used to draw the sample from the bottom of the cuvette, and the other tube served as ventilation to prevent the creation of a vacuum. The sample was immediately injected into the sparge tube of the GC. Separate samples for initial DMS concentration were drawn from the same quartz tube used to fill the cell just prior to and following the GC analysis of the incubated sample.

For each water sample, from 10 to 12 wavelengths were examined, and each wavelength was irradiated at least in duplicate. The amount of DMS photolyzed during an irradiation ranged from 3 to 25% of the initial DMS concentration. Parallel dark samples were examined to account for any DMS loss associated with the experimental setup. Leakage through the Teflon stopper and other dark processes accounted for a DMS loss of  $\sim 2\%$  over 16.5 h. Most incubation times ranged from 20 to 180 min, so dark loss was negligible, but all quantum yield determinations were corrected for this loss.

Once photolysis rates were determined, quantum yields were then calculated. Absolute quantum yields could not be determined, however, because as stated previously, the photosensitizers for DMS photolysis are not known. Therefore, the apparent quantum yield was determined as

$$\Phi_{\text{PO}}(\lambda) = \frac{d(\text{DMS})_{\lambda} V}{P_{\lambda}(1 - 10^{-A_{\lambda}})} \quad (2)$$

where  $\Phi_{\text{PO}}(\lambda)$  is the wavelength-dependent apparent quantum yield for DMS photolysis,  $d(\text{DMS})_{\lambda}/dt$  is the wavelength-specific photolysis rate for DMS ( $\text{mol DMS L}^{-1} \text{ s}^{-1}$ ),  $V$  is

the volume of seawater irradiated (liters),  $P_{\lambda}$  is the radiant flux ( $\text{mol photons s}^{-1}$ ), and  $A_{\lambda}$  is the absorbance, with  $(1 - 10^{-A_{\lambda}})$  representing the fraction of incident radiation absorbed by CDOM. The photon flux in the 1-cm quartz cell was determined using nitrite chemical actinometry (Jankowski et al. 1999; Jankowski et al. 2000). The apparent quantum yield for photolysis represents a minimum estimate of the true quantum yield, since it is likely that only a fraction of CDOM photosensitizes the photolysis of DMS in seawater.

*Polychromatic rooftop incubations*—To verify the wavelength regions primarily responsible for DMS photolysis, polychromatic rooftop incubations were performed using ambient sunlight and broadband cutoff filters. The 15- and 80-m seawater samples were exposed to solar radiation on 7–8 (15 m) and 11–12 August 2001 (80 m) on the roof of the laboratory in Syracuse, New York. Specifically designed, Teflon-sealed quartz tubes (Kieber et al. 1997) containing  $\sim 20 \text{ nmol L}^{-1}$  DMS in 0.2- $\mu\text{m}$ -filtered seawater were placed in a shallow, circulating, freshwater bath at 20°C. The water bath was placed on a flat black background to minimize scattered or reflected light. Duplicate quartz tubes were subjected to different spectral irradiances using long-pass filters of Mylar D polyester film and UF3-plexiglas with cutoffs at 313 and 400 nm (see Miller 2000, for transmission spectra), approximating a UV-B (280–320 nm) and a total UV filter, respectively. DMS photolysis in these spectral treatments was compared to samples exposed to the entire solar spectrum in quartz tubes and to dark controls wrapped in aluminum foil. Initial DMS concentrations were determined in all samples prior to rooftop deployment. Quartz tubes were rotated in the water bath hourly to minimize differences due to sample location. CDOM absorption spectra were determined in all quartz tubes initially and at the conclusion of each incubation.

## Results

*Quantum yield determinations*—For both the 15- and 80-m seawater samples, wavelength-dependent apparent quantum yields decreased exponentially with increasing wavelength in the UV (Fig. 3A,B). The quantum yield spectra were accurately described by simple exponential functions determined from nonlinear least squares regression (290–380 nm,  $r^2 = 0.96$  for 15 m; 290–410 nm,  $r^2 = 0.98$  for 80 m).

$$\Phi_{\text{PO}}(\lambda, 15 \text{ m}) = (\text{DMS})31.9e^{-0.0499\lambda} \quad (3)$$

$$\Phi_{\text{PO}}(\lambda, 80 \text{ m}) = (\text{DMS})0.10e^{-0.0321\lambda} \quad (4)$$

The 15-m sample, characterized by lower CDOM absorption, had significantly higher apparent quantum yields (at the 95% CI) in the UV-B compared with the 80-m sample. This indicates that the mixed-layer sample (15 m) is more effective on a per-photon-absorbed basis for shorter UV wavelengths (<320 nm), whereas the deeper sample (80 m) is more effective at longer UV wavelengths (>360 nm, Fig. 3C). Although this spectral shape is fairly characteristic of photochemical processes in seawater (e.g., Neale and Kieber

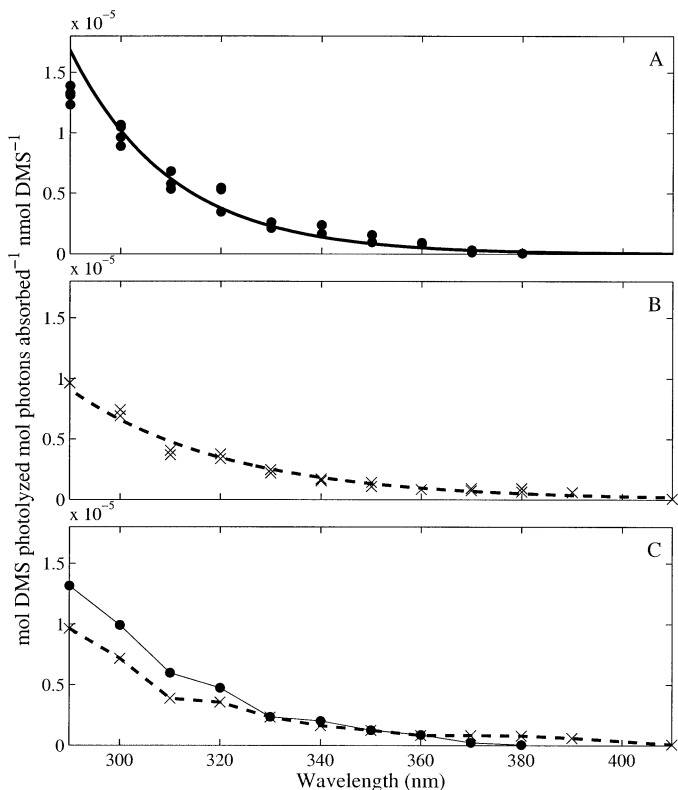


Fig. 3. Wavelength-resolved apparent quantum yields of DMS photolysis for (A) the 15-m sample and (B) the 80-m sample (mol DMS photolyzed per mol photon absorbed by CDOM per nmol DMS). In panels A and B, the circles and crosses, respectively, are replicates and the solid line and dashed lines, respectively, are the best fit exponential curves. (C) Mean spectral DMS quantum yields for the 15- and 80-m samples (symbols remain the same). Determinations were made at 21°C.

2000), the observed slopes are high compared to apparent quantum yield slopes for other photochemical reactions in the open ocean. These slopes range from 0.0250 to 0.0271 nm<sup>-1</sup> for the production of carbon monoxide (Nelson unpubl. data), 0.0120 to 0.0272 nm<sup>-1</sup> for the production of hydrogen peroxide (Miller 2000; Yocis et al. 2000), 0.0398 nm<sup>-1</sup> for the production of carbon disulfide (Xie et al. 1998), and 0.0288 nm<sup>-1</sup> for the production of carbonyl sulfide (Weiss et al. 1995). The slopes of the quantum yield functions (0.0499 and 0.0321 nm<sup>-1</sup> for the 15- and 80-m samples, respectively) were also much steeper than the corresponding slopes for the CDOM absorption coefficients (290–350 nm, 0.0208 and 0.0181 nm<sup>-1</sup> for the 15- and 80-m samples, respectively). This indicates that on a per-photon basis, shorter UV-absorbing chromophores are more effective in driving DMS photolysis than longer wavelength-absorbing chromophores.

Reciprocity studies were conducted to insure that the incubations for the quantum yield determinations were sampled during the period where photolysis is a linear function of photon exposure (Neale and Kieber 2000). For these experiments, separate seawater samples were irradiated for specific time intervals, generally ranging between 0 and 90 min. For example, the photolysis of DMS in the 80-m water sam-

ple at 320 nm was a linear function of light dose up to 90 min, after which, rates were nonlinear, presumably because of photobleaching of the DOM photosensitizer(s) (data not shown). In addition, to ascertain whether bleaching of CDOM was important during monochromatic irradiations, seawater samples were irradiated with no added DMS, at the same wavelengths and time intervals used for apparent quantum yield incubations, to monitor changes in the CDOM absorption coefficients. For both the 15- and 80-m samples and for all wavelengths, no statistically significant changes in CDOM absorption were observed relative to dark controls (<5% differences were noted for the entire absorption spectrum). Because CDOM absorption coefficients did not change during monochromatic irradiations, it was assumed that concentrations of the components of CDOM related to DMS photolysis also did not significantly change. For both samples and at all wavelengths, quantum yields were determined in the linear region where reciprocity was observed (i.e., apparent quantum yields were constant).

*Temperature dependence*—In addition to its wavelength dependence, the rate of DMS photolysis was temperature dependent. Temperature dependence studies were conducted on both water samples at 320 nm and at temperatures ranging from 4.9 to 34.5°C. DMS photolysis rates increased exponentially with increasing temperature following simple Arrhenius behavior (Fig. 4A,B). Simple exponential relationships derived from nonlinear least squares regression described the temperature dependence ( $r^2 = 0.96$  for 15 m;  $r^2 = 0.98$  for 80 m).

$$\frac{d(\text{DMS})}{dt} = 0.00165e^{0.0319T} \quad (5)$$

$$\frac{d(\text{DMS})}{dt} = 0.00185e^{0.0351T} \quad (6)$$

$T$  is temperature (°C), and the pre-exponential constant corresponds to a DMS concentration of 1 nmol L<sup>-1</sup>. Over the temperature range studied, the quantum yield increased by a factor of 2.72 and 2.83 for the 15- and 80-m samples, respectively, resulting in an approximate doubling of quantum yields for an increase of 20°C. Activation energies for the photolysis of DMS, determined from the Arrhenius plots, were  $22.7 \pm 1.2$  and  $24.8 \pm 1.9$  kJ mol<sup>-1</sup> for the 15- and 80-m samples, respectively (Fig. 4A,B insets). For modeling purposes, although it was not explicitly verified here, these temperature relationships were assumed constant across all wavelengths.

*Polychromatic rooftop experiments*—Photolysis rates for both the 15- and 80-m samples were greatest in the untreated quartz tubes as compared to the Mylar and UF3-plexiglas treatments. On the basis of differences between light treatments, maximum photolysis rates were observed in the UV-A (320–400 nm). In the 15-m sample, characterized by lower CDOM absorption coefficients, the UV-B was responsible for 38.8% of the photolysis, with UV-A wavelengths accounting for 61.2% (Fig. 5A). The 80-m sample, with the higher CDOM absorption, was ~50% less sensitive to UV-B radiation, with UV-B wavelengths accounting for only

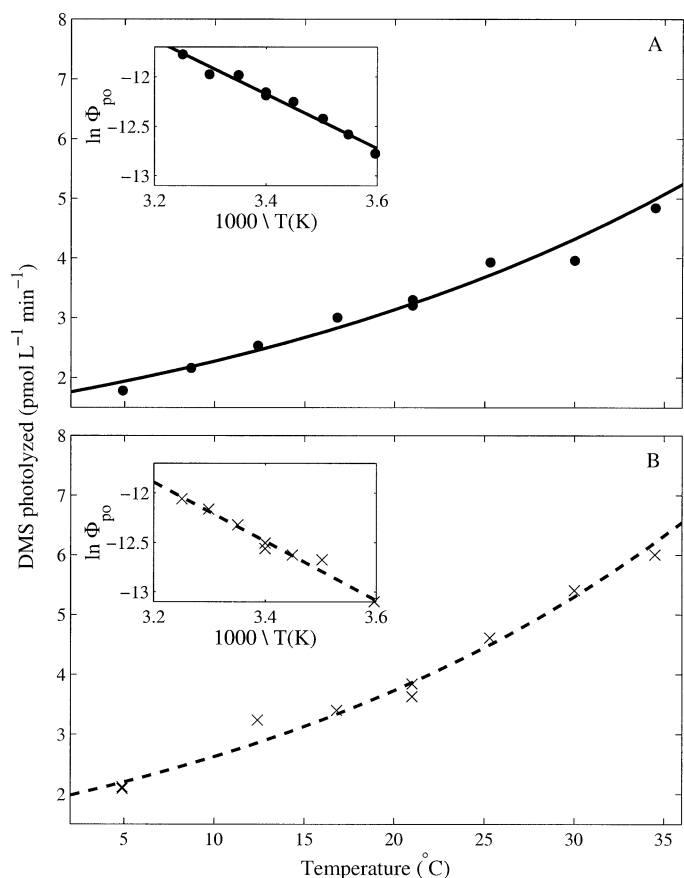


Fig. 4. Temperature dependence of DMS photolysis rates for (A) the 15-m sample and (B) the 80-m sample. Rates are scaled to an initial DMS concentration of  $1 \text{ nmol L}^{-1}$ . The inset Arrhenius plots are the natural log of calculated quantum yields derived from the temperature dependence experiments versus  $1,000$  divided by temperature in Kelvin.

20.4% of the photolysis and UV-A responsible for the remaining 79.6% (Fig. 5B). In addition, over the duration of the 2-d incubation, approximately three times as much DMS was photolyzed in the 80-m sample versus the 15-m sample. Unfortunately, concurrent irradiance measurements were not available during these incubations. To eliminate this as a source of the observed differences, new aliquots of the 15- and 80-m samples were exposed to solar radiation on the same days, focusing solely on the UV wavelength region (14–15 August 2001). These incubations yielded quantitatively similar results to those observed in the initial rooftop irradiation experiments and confirmed the higher rates in the 80-m sample, consistent with the higher CDOM absorption coefficients and higher apparent quantum yields in the UV-A (Fig. 3). Rates were approximately 2.5-fold higher in the 80-m sample, and the UV-B and UV-A wavelength regions were responsible for 35.5 and 64.5% and 19.2 and 80.8% of the DMS photolysis for the 15- and 80-m samples, respectively. Although some degree of nonlinearity is expected because the production and loss of DMS photolysis precursors does not necessarily parallel that of bulk CDOM, the observed wavelength partitioning was likely a result of differences in photosensitizer concentrations, as suggested by the

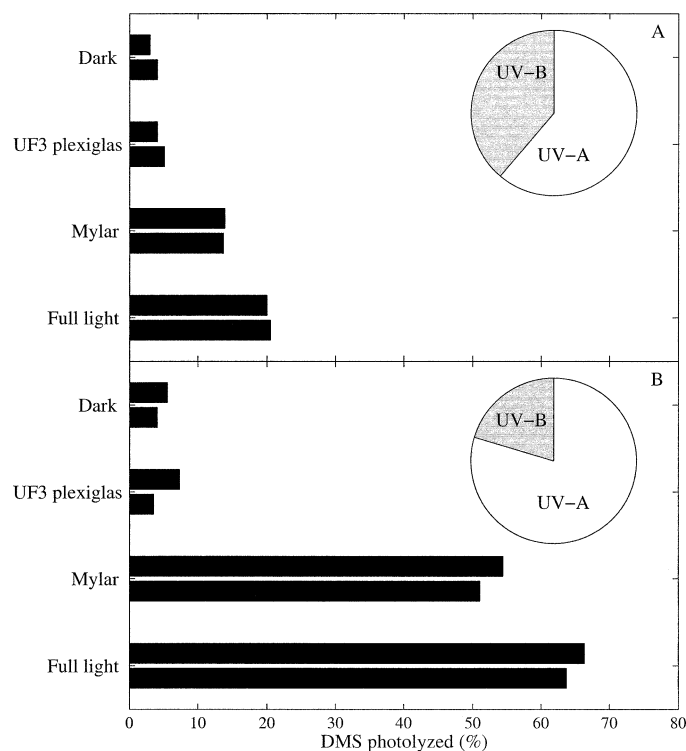


Fig. 5. Percentage of initial DMS photolyzed during the polychromatic broadband rooftop experiments using natural sunlight for (A) the 15-m sample and (B) the 80-m sample. All treatments were in duplicate, and the inlaid pie charts are approximate spectral partitioning of UV-B (280–320 nm) and UV-A (320–400 nm) contributions to the total photolysis based on differences between the various light treatments. UV-B accounted for 38.8 and 20.4% and UV-A for 61.2 and 79.6% of the total photolysis for the 15- and 80-m samples, respectively.

higher CDOM absorption coefficients in the 80-m water sample (Fig. 2), and photosensitizer quality, as reflected in initial slope factors ( $0.0208 \text{ nm}^{-1}$  for 15 m vs.  $0.0181 \text{ nm}^{-1}$  for 80 m) (Green and Blough 1994; Nelson et al. 1998).

For all rooftop incubations, the differences between the dark replicates and the replicates incubated under UF3-plexiglas were statistically insignificant ( $<5\%$ ) indicating that DMS photolysis does not occur at wavelengths greater than  $\sim 400 \text{ nm}$  in Sargasso Sea seawater (Fig. 5). This finding differs from previous results from the Pacific which, employing identical techniques to determine action spectra as those used in the present study, showed significant photolysis rates in the visible portion of the solar spectrum (Kieber et al. 1996). Sample storage artifacts associated with Pacific seawater cannot be ruled out, however, since the  $0.2\text{-}\mu\text{m}$ -filtered Pacific samples used in laboratory studies were stored refrigerated in Teflon-lined polyethylene bottles for more than a month. Although this is unlikely, as shipboard photolysis experiments using freshly collected samples showed no attenuation of photolysis rates in polycarbonate enclosures with a 365-nm cutoff, it might have contributed to the observed differences between the Sargasso Sea and Pacific action spectra.

**Photolysis rates**—As mentioned previously, the depth-dependent DMS photolysis rate,  $PO(z)$ , is defined as the product of the photolysis quantum yield  $\Phi_{PO}$  and the absorbed quanta  $AQ(z, \lambda, t)$ ,

$$PO(z) = \int_t \int_z \int_\lambda \Phi_{PO}(\lambda) AQ(z, \lambda, t) dt dz d\lambda$$

$$= \int_t \int_z \int_\lambda \Phi_{PO}(\lambda) a_{CDOM}(z, \lambda) E_0(z, \lambda, t) \frac{\lambda}{hc} dt dz d\lambda \quad (7)$$

where  $a_{CDOM}(z, \lambda)$  is the spectral CDOM absorption coefficient,  $E_0(z, \lambda, t)$  is the depth-dependent spectral scalar irradiance integrated over 1 d,  $h$  is Planck's constant,  $c$  is the speed of light in a vacuum, and  $\lambda/hc$  converts the photon flux at a given wavelength to energy. Following Eq. 7, depth-dependent photolysis rates were determined by combining the monochromator-determined quantum yields, measured CDOM absorption coefficients, and a measure of the spectral scalar irradiance. In this case, a monthly UV climatology determined from atmospheric radiative transfer calculations (including column-integrated ozone abundance and climatological cloud properties) was applied (*see* Lubin et al. 1998). The downward irradiance was converted to scalar irradiance assuming a conversion factor of 1.2. On the basis of underwater radiative transfer simulations for the upper 5 m, a solar zenith angle of  $30^\circ$ , clear skies, and the wavelength range of maximum photolysis activity (300–380 nm), the conversion factor varied from 1.15–1.17 in the summer to 1.16–1.24 in the winter. For completely diffuse conditions, the conversion factor ranged from 1.21–1.24 in the summer to 1.22–1.29 in the winter. These simulations were carried out for extreme cases in the Sargasso Sea; thus, these ranges can be considered outer bounds for the planar to scalar irradiance conversion factor at this site. Although this factor does vary as a function of wavelength, depth, sky state, and the inherent optical properties of the water column, 1.2 is a reasonable average value (HYDROLIGHT, Mobley 1994; Nelson unpubl. data).

Using these calculations, DMS photolysis rates were determined for the upper cubic meter of the water column and as a function of depth in the water column (*see Discussion*). Modeled surface DMS photolysis rates were extremely low at 290 and 300 nm because of the low solar flux at these wavelengths and increased to a maximum at 320 nm, followed by a decrease with increasing wavelength (Fig. 6). Although the 80-m sample is characterized by lower quantum yields at shorter wavelengths ( $<360$  nm), when the same scalar irradiance was applied, the higher CDOM absorption dominated, resulting in a larger photolysis rate for all wavelengths. Integration of the area under the curves shown in Fig. 6 indicated that the photolysis rate for the 80-m samples was 175% higher than that determined for the 15-m sample, approximating results obtained in the rooftop studies, which suggested a 2.5-fold difference between samples. Additionally, integration showed that UV-B and UV-A accounted for 32.6 and 67.4% of the photolysis for the 15-m sample and 22.2 and 77.8% of the photolysis for the 80-m sample. This spectral partitioning of the active photolysis

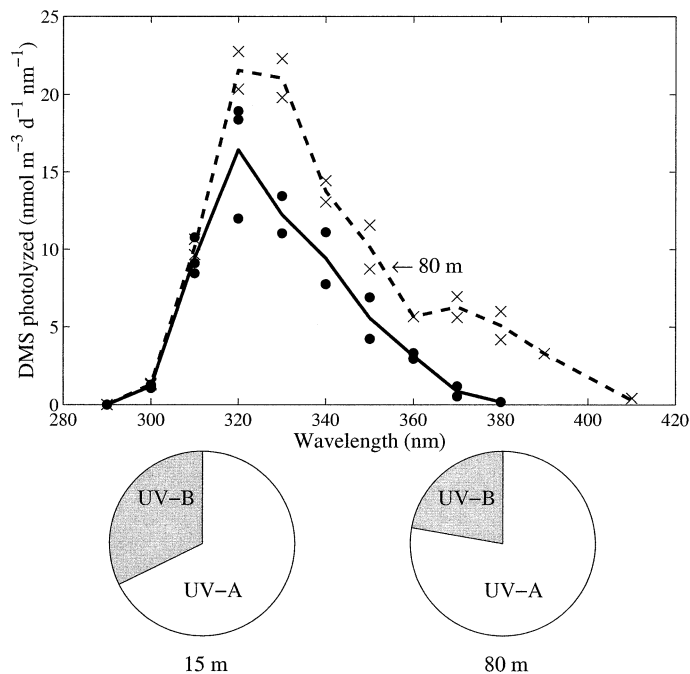


Fig. 6. Wavelength-resolved surface photolysis rates for the 15- and the 80-m seawater samples. Photolysis rates were determined using Eq. 7, mean measured quantum yields, sample-specific  $a_{CDOM}(\lambda)$ , and a regionally specific climatological UV incident flux (Lubin et al. 1998). Quantum yield spectra were scaled to an initial DMS concentration of  $1 \text{ nmol L}^{-1}$  and  $21^\circ\text{C}$ . Pie charts are the approximate spectral partitioning of UV-B (280–320 nm) and UV-A (320–400 nm) contributions to the total photolysis based on integration of the photolysis rates. UV-B accounted for 32.6 and 22.2% and UV-A for 67.4 and 77.8% of the total photolysis for the 15- and 80-m samples, respectively.

region matched that observed in the rooftop experiments under natural solar radiation (38.8 and 61.2% for the UV-B and UV-A, respectively, in the 15-m samples and 20.4 and 79.6% for the 80-m sample), verifying our monochromator results.

## Discussion

**Seasonal cycle modeling**—The Dacey et al. (1998) DMS time series (1992–1994) provides a clear example of the summer paradox (Fig. 1A–C). To assess the role of photolysis in this phenomenon, photolysis rates were examined in space and time in conjunction with the various forcing factors. Following Eq. 7, depth-integrated photolysis rates were determined by combining (1) the laboratory-measured apparent quantum yields of photolysis, (2) spectral CDOM absorption coefficients as a function of depth, (3) spectral incident irradiance and diffuse attenuation coefficients as a function of depth, and (4) the monthly resolved time series of DMS concentrations. All photolysis calculations were integrated to the base of the seasonal mixed layer derived from same-day CTD casts and over one day length. The calculations implicitly assumed that the concentration of DMS and the CDOM absorption coefficients remained constant over 1 d.

Table 1. Estimated seasonal DMS photolysis rates and specific turnover rates. Photolysis rates are integrated to the base of the surface mixed layer. Summer is defined as 1 May–30 Sep.

Case	$E_0(\lambda, z)$	$a_{\text{CDOM}}(\lambda)$	Photolysis rate ( $\mu\text{mol DMS m}^{-2} \text{d}^{-1}$ )		Turnover rate ( $\text{d}^{-1}$ )	
			Summer	Nonsummer	Summer	Nonsummer
1	BATS reconstructed	UCSB inversion model	3.8–16.8	0.6–5.5	0.05–0.22	0.01–0.12
2	BATS reconstructed	1995–2001 BATS climatology	4.2–24.5	0.4–8.9	0.06–0.29	0.01–0.19
3	Lubin et al. climatology	UCSB inversion model	5.3–15.6	0.5–6.5	0.06–0.21	0.01–0.14
4	Lubin et al. climatology	1995–2001 BATS climatology	5.5–22.9	0.4–10.7	0.09–0.29	0.01–0.20

CDOM absorption coefficients, incident UV flux, and underwater UV profiles were not taken concurrently with the DMS time series and were therefore modeled. As a sensitivity analysis to assess how the calculation procedures affected the final photolysis rates, and thus the overall robustness of the results, several parallel calculations were carried out. These calculations included two independent CDOM absorption coefficient parameterizations and two incident irradiance parameterizations. Results of this comparison are shown in Table 1. Furthermore, DMS apparent quantum yields (Eqs. 3, 4) were scaled to temperature (Eqs. 5, 6) and ambient DMS concentrations. Separate model calculations were performed using the apparent quantum yield spectra from the 15- and 80-m samples to mimic the range of CDOM qualities expected in the Sargasso Sea.

*CDOM modeling*—CDOM absorption coefficients were modeled using a 7-yr mean of measurements at this site and derived from a semianalytical ocean color inversion model. Beginning in 1995, as part of the Bermuda Bio-Optics project (BBOP) program, CDOM measurements were collected approximately 16 to 20 times a year in the upper 140 m (Nelson et al. 1998). Although there is considerable inter-annual variability, a depth-resolved seasonal composite of all available data from 1995–2001 was created, yielding the well-documented temporal and spatial patterns (Nelson et al. 1998; Nelson and Siegel 2002). CDOM absorption is generally lowest in the summer in the mixed layer when stratification is strongest and bleaching occurs. It is highest at depth in the summer because of high local production rates and is fairly homogeneous with depth in the winter because of physical mixing processes, low biological activity, and low UV fluxes (Siegel and Michaels 1996; Nelson et al. 1998).

CDOM absorption was also modeled using the globally optimized semianalytical University of California–Santa Barbara (UCSB) inherent optical property (IOP) ocean color inversion model (Maritorena et al. 2002). Using remote sensing reflectances at wavelengths 412, 443, 490, 510, and 555 nm, this model estimates surface CDOM and detrital absorption at a wavelength of 443 nm, particulate backscattering at a wavelength of 443 nm, and Chl *a* concentrations. Underwater profiles of downwelling irradiance and upwelling radiance were determined from near-noon optical casts sampled by the Marine Environmental Radiometer package (Biospherical Instruments; Siegel et al. 2001). The optical profiles were extrapolated to and across the air–sea interface, providing remote sensing reflectances. CDOM absorption

was extended spectrally using Eq. 1 and a spectral slope of  $0.0206 \text{ nm}^{-1}$ , which was found to produce the most consistent results when tuned globally (Maritorena et al. 2002). In this case, CDOM absorption was considered constant within the mixed layer.

In both CDOM parameterizations, the absorption coefficients were considered constant over the time course of 1 d. Although the concentration of chromophoric DMS photolysis precursors might change during this time period as the reaction progresses, without knowledge of the exact reaction photosensitizers or the reaction mechanism, it is impossible to model this change. Nelson et al. (1998) demonstrated that bulk CDOM in the Sargasso Sea has a lifetime of approximately 90 d with respect to photobleaching processes and 14 d with respect to bacterial production processes, suggesting that this was a reasonable assumption.

*Irradiance modeling*—The incident dose (i.e., time-integrated irradiance) was modeled via (1) a literature UV climatology and (2) irradiance reconstructed from measured visible fluxes. The first method consisted of using a spectral incident irradiance  $1^\circ \times 1^\circ$  monthly UV climatology (Lubin et al. 1998). The second downwelling UV flux estimate was constructed from shipboard measurements of nearly concurrent ( $\pm 2$  d) measured daily integrated visible irradiances. Relying on climatological results is not prudent because this site experiences considerable deviation in daily incident irradiance because of cloud variability (Siegel et al. 2001; Fig. 1D). During core BATS cruises from August 2000 to November 2001, a deck-mounted cosine-corrected radiometer sampled throughout the day, allowing for the development of empirical relationships between daily integrated UV and visible irradiances. Ratios between integrated UV irradiance and integrated visible irradiance at 412 nm were surprisingly constant throughout the 15-month period, at  $0.305 \pm 0.017$  (SD) for 324 nm,  $0.451 \pm 0.016$  for 340 nm, and  $0.542 \pm 0.015$  for 380 nm. Applying these ratios to daily integrated  $E_d(412)$  measurements from the original sampling period, a time series of integrated irradiance at 324, 340, and 380 nm was reconstructed. Extrapolation to other UV wavelengths was based on inter-UV wavelength ratios derived from the Lubin et al. (1998) climatology. These ratios were constant throughout the year and matched up with similar ratios from the BBOP 2000–2001 dataset quite well. For example, the Lubin et al. (1998) climatology has a mean  $E_d(324)/E_d(340)$  ratio of  $0.703 \pm 0.012$ , whereas the mean BBOP  $E_d(324)/E_d(340)$  ratio was  $0.677 \pm 0.022$ . This reconstruction allowed the modeled incident light fields to more accurately

reflect the solar conditions on the day the time series seawater samples were collected.

Depth-dependent irradiance was estimated from diffuse attenuation coefficients, which can be related to the absorption and scattering coefficients (Kirk 1981).

$$K_d(\lambda) = \sqrt{a(\lambda)^2 + 0.231a(\lambda)b(\lambda)} \quad (8)$$

$K_d(\lambda)$  is the downwelling diffuse attenuation coefficient,  $a(\lambda)$  is the spectral total absorption coefficient, and  $b(\lambda)$  is the spectral total scattering coefficient. Total scattering coefficients were derived as a function of chlorophyll concentrations (Fig. 1C) using a basic bio-optical model (Gordon and Morel 1983). Absorption by pure water was extended into the UV assuming that the spectral slope for wavelengths 380–410 nm remained constant to 290 nm (using data from Pope and Fry 1997). During core BATS cruises from August 1999 to December 2001, profiles of UV irradiance and radiance were sampled, allowing for the development of an empirical absorption parameterization. It was found that approximating total absorption as the sum of absorption by pure water and absorption by CDOM determined from the Maritorena et al. (2002) retrievals, extended spectrally with a lower  $S$  factor ( $0.0194 \text{ m}^{-1}$ ) (Eq. 1), combined with scattering following Eq. 8 yielded the most accurate  $K_d(\lambda)$  spectrally (modeled vs. measured  $K_d(\lambda)$ ,  $r^2 = 0.94$  for  $\lambda \leq 412$  nm, slope = 1.001, intercept =  $-0.003$ ,  $n = 33$  profiles).

*Seasonal photolysis rates and turnover times*—Apparent quantum yield spectra, along with modeled CDOM absorption, modeled underwater irradiance fields, and the time series of DMS concentrations and temperature were used to calculate depth-integrated photolysis rates following Eq. 7. Figure 7A shows an example of mixed-layer integrated photolysis rates based on the CDOM absorption derived from the ocean color inversion estimates and the incident UV reconstructed from BATS data (Table 1, case 1). Peak summertime photolysis rates were greater than  $16 \mu\text{mol DMS m}^{-2} \text{ d}^{-1}$ , whereas midwinter photolysis rates were  $< 1 \mu\text{mol DMS m}^{-2} \text{ d}^{-1}$ . Corresponding specific turnover rates in the summer ranged from  $0.05$  to  $0.22 \text{ d}^{-1}$  and as low as  $0.01 \text{ d}^{-1}$  in the winter (Fig. 7B). Use of the climatological  $a_{\text{CDOM}}(z, \lambda)$  lead to relatively higher photolysis rates and a proportional increase in specific turnover rates because of a variety of factors (Table 1, case 2, 4 vs. case 1, 3). First, the ocean color inversion parameterization does not take into account seasonal variations in the CDOM absorption exponential slope parameter  $S$  and assumes that one factor holds throughout the entire UV wavelength region. Log-transformed CDOM absorption spectra deviate from linearity in the shorter UV wavelengths, suggesting a larger  $S$  factor for shorter wavelengths and thus a relative underestimation by the ocean color inversion model. In addition, because of the high degree of interannual variability associated with CDOM absorption measurements, a 7-yr mean will not necessarily be representative of the actual CDOM absorption during 1992–1994. Use of the Lubin et al. (1998) monthly climatological UV dataset tended to slightly overestimate the downwelling irradiance relative to the BATS reconstructed

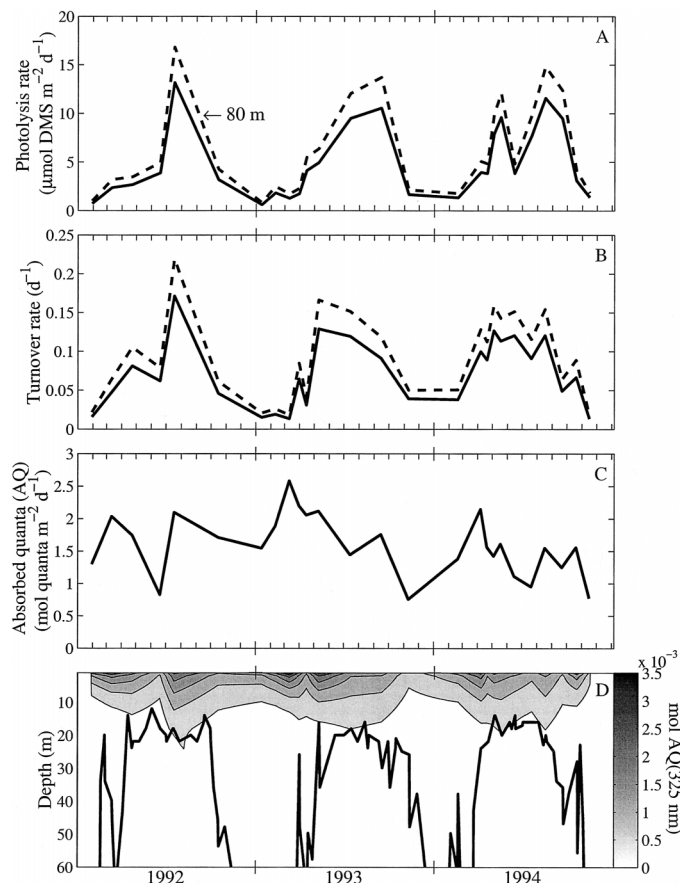


Fig. 7. (A) Mixed-layer, depth-integrated DMS photolysis rates for the 15- and 80-m sample, (B) specific turnover rates in the surface mixed layer calculated as photolysis rate divided by mixed-layer integrated DMS concentration, (C) total absorbed quanta (290–400 nm) that is the product of  $a_{\text{CDOM}}(\lambda)$  and  $E_0(\lambda, z)$ , and (D) contours of depth-resolved absorbed quanta at 325 nm overlaid with mixed-layer depth (thick solid line). These calculations were carried out using the globally optimized semianalytical UCSB IOP inversion model (Maritorena et al. 2002) and incident UV reconstructed from the BATS visible dataset (Table 1, case 1).

estimates, producing increased photolysis rates and larger specific turnover times (Table 1, case 3, 4 vs. case 1, 2).

Qualitatively, the results are robust; the different calculations all indicate the same seasonal pattern. For all calculations, the difference between the summer maximum and winter minimum in DMS photolysis rates was approximately 30-fold, whereas differences from the use of the two apparent quantum yields was only 20 to 35%. Most likely, the mixed-layer photolysis rates resemble those derived from the 15-m quantum yield in the summer, when the water column is extremely stratified, and those calculated from the 80-m quantum yield in the winter, when deep convective mixing results in deeper sources of higher absorbing CDOM.

The pattern of DMS photolysis rates observed in Fig. 7 is primarily due to seasonal changes in DMS concentrations, seawater temperature, and the incident irradiance. Because DMS photolysis is a pseudo-first-order reaction, wavelength-dependent quantum yields are directly proportional to ambient DMS concentrations, which vary by a factor of  $> 12$

seasonally (Fig. 1A). The quantum yields also scale to the in situ temperature following Eqs. 5 and 6. Sea surface temperatures are cold (19–22°C) and homogeneous with depth in the winter and warm to a maximum of 27–30°C during the spring and the summer. If all other factors remained constant, the increase in temperature from the winter to the summer would result in an ~40% increase in summer DMS photolysis rates.

Mixed-layer integrated absorbed quanta were also slightly higher in the summer, reflecting the balance between increased incident irradiance, lower CDOM absorption, and shallower mixed-layer depths (Fig. 7C). Essentially, the absorbed quanta are the product of the fraction of light absorbed by CDOM and the incident irradiance in the mixed layer and will thus be affected by seasonal variations in the intensity and spectral distribution of actinic solar radiation in the water column. In the Sargasso Sea, CDOM absorption coefficients are roughly two to three times lower in the summer (Fig. 1E) as the CDOM bleaches through UV exposure, reducing its photosensitizing ability and permitting deeper penetration of UV radiation. At the same time however, the incident UV irradiance concurrently increases two to three times depending on meteorological conditions (Fig. 1D). While the mixed-layer depth mirrors the seasonal temperature progression, ranging from >150 m in the winter to depths as shallow as 15–20 m in the summer, its effect on integrated absorbed quanta, and thus photolysis rates, is minimal (Fig. 7D). In the summertime, although UV wavelengths are not necessarily 100% absorbed in the surface mixed layer, because of the exponential attenuation of light, an appreciable percentage are (Fig. 7D). During the winter, when mixed layers are very deep (>150 m), UV wavelengths are essentially 100% absorbed. Thus, there is very little seasonal difference in the degree to which UV radiation is absorbed within the surface mixed layer. Seasonal differences in the integrated absorbed quanta are primarily dominated by seasonal variations in the availability of UV irradiance damped by lower CDOM absorption. The result is slightly elevated, integrated mixed-layer absorbed quanta in the summertime, driving higher DMS photolysis rates.

Seasonal changes in CDOM absorption coefficients will affect the depth horizon over which UV photons are attenuated, however. Radiometer casts (SPMR, Atlantic) taken concurrently with the initial seawater sampling indicated that the 1% light level for 324 nm, approximately the wavelength of maximum photolysis, was 42 m, and the 1% light level for 412 nm was 93 m (Fig. 8). Summertime in the Sargasso Sea is characterized by some of the optically clearest seawater worldwide, so these 1% light levels can be considered upper bounds for the depth over which photolysis occurs. In general, even in the clearest open ocean waters, UV radiation is exponentially attenuated in the upper 20 or 30 m, and consequently, the majority of absorbed quanta and water column DMS photolysis occurs at these shallow depths. As shorter wavelengths of light are attenuated preferentially, the spectral composition of in situ UV light will shift to longer wavelengths. Therefore, as depth increases, fewer total photons are present and there is a simultaneous shift to longer wavelengths characterized by lower quantum yields and lower CDOM absorption. The net result is that fewer photons

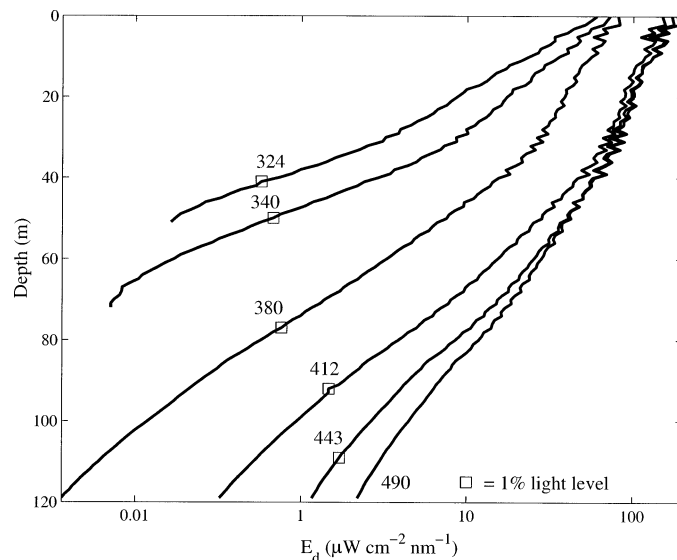


Fig. 8. Attenuation of downwelling irradiance,  $E_d(\lambda)$  with depth, from the cast just prior to water sample collection on 19 July 2001 (wavelengths are noted next to each irradiance profile). One percent light levels are noted with square markers. Radiometric measurements were collected using a SeaWiFS profiling multichannel radiometer (SPMR).

are absorbed and less DMS photolysis occurs per photon absorbed.

*Implications for the summer paradox*—Calculations presented here demonstrated that DMS photolysis peaks in the summer, concurrent with larger incident UV irradiance, temperatures, and in situ concentrations of DMS. They also indicate that photolysis is not the main factor controlling the DMS summer paradox. If photolysis controlled mixed-layer DMS concentrations, one would expect DMS concentrations to be lowest during the summer and this is exactly opposite of what is observed in this region. Photolysis contributes to the dampening of DMS concentrations in the upper water column (<20 m) but cannot explain the large midsummer buildup deeper in the water column. Clearly, other mechanisms must lead to the elevated DMS concentrations in the summer. Seasonal changes in wind-driven sea-air losses of DMS cannot explain this trend because atmospheric ventilation is at a maximum in the summer because of increased DMS concentration gradients between the ocean and the boundary layer and increased oceanic temperatures (*see discussion below*). Chemical oxidation of DMS is also negligible because DMS has residence times on the order of years with respect to that process (Shooter and Brimblecombe 1989). Ultimately, with abiological losses eliminated as the primary drivers of the observed pattern of DMS concentrations, there are two, potentially interacting, light-driven processes driving the summer paradox: either a reduction in bacterial consumption of DMS (e.g., Herndl et al. 1993) or an increase in DMS production by bacteria or phytoplankton (e.g., Sunda et al. 2002) or both. To gain an insight into the observed pattern and forcing mechanisms, we can draw from

many of the previous studies that have focused on specific elements of the sulfur cycle and their relationship with light.

One possibility for the summer paradox is a reduction in summertime bacterial DMS consumption rates. Ultraviolet radiation is capable of transforming refractory DOM into more labile forms stimulating bacterial activity (Kieber 2000). In addition, CDOM is produced locally as a by-product of microbial metabolism (Nelson et al. 1998; Nelson and Siegel 2002). Seasonal changes in CDOM concentration and composition can lead to changes in bacterial activity that presumably affect DMS bacterial consumption (Kiene and Bates 1990). Experimentally, Slezak et al. (2001) demonstrated that, under surface irradiance conditions, microbial removal of DMS was inhibited by  $59.6 \pm 14.0\%$  ( $\pm$ SD) versus dark controls. They found that various spectral regions had differential inhibitory effects on bacterial consumption of DMS, supporting the importance of the spectral quality of light as modulated by CDOM absorption. In addition, although bacterial abundance is rather invariable, certain subpopulations are highly seasonal, making it difficult to generalize literature consumption rates. Supporting this, Slezak et al. (2001) noted high spatial and temporal variability in bacterial sensitivity to solar irradiation. Depending on the quantity and quality of CDOM, the spectral shape of the downwelling irradiance, and the speciation and sensitivity of the bacterial population, a buildup of DMS could occur as bacterial consumption is inhibited by the seasonal increase in the clarity of the water column from the winter to the summer.

Under conditions of inhibition from increased UV radiation, bacterial sulfur demands could be less, suggesting changes in how DMSP is processed. Bacterial populations assimilate DMSP as a source of reduced sulfur for protein synthesis (e.g., Kiene et al. 1999). Kiene et al. (2000) found that the microbial conversion rate is dependent on DMSP concentration and bacterial demand. They observed that at higher DMSP concentrations, a lower fraction of DMSP was assimilated, with a larger portion being converted to DMS as bacterial sulfur demands were satisfied. Bacterial sulfur demands depend on the biomass, growth rate, and composition of the bacterial community in the water column. Their community composition and activity can be affected to considerable depths, however, depending on the light regime, further complicating direct interpretation of past results (e.g., Herndl et al. 1993; Simó and Pedrós-Alió 1999a).

Another plausible explanation for the DMS summer paradox is that increased UV radiation in the summertime results in an increase in the phytoplankton conversion rate of DMSP to DMS. Changes in either the spectral intensity or composition of incident radiation will affect the balance between the biological production of DMSP by phytoplankton and the subsequent conversion to DMS. A summertime increase in DMS in conjunction with increased water clarity and irradiance is consistent with the antioxidant function of DMSP and DMS demonstrated by Sunda et al. (2002). As oxidative stressors such as UV radiation increase, intracellular phytoplankton production of DMSP and its resulting enzymatic cleavage to DMS is expected to increase. Sunda et al. (2002) found that the greatest accumulation of DMS and DMSP per cell volume was observed at intermediate

levels of UV stress. At higher levels of UV stress (full UV-B exposure), the overall metabolic production of DMSP and DMS is expected to be greater, but the oxidative removal should also be faster, resulting in lower net cellular DMSP concentrations relative to levels observed under intermediate UV stress. Although it might result from a variety of concurrent factors, the midwater column maximum (20–40 m) in DMS evident in the time series is consistent with the antioxidant hypothesis.

Increased DMSP and DMS production in the summer might also be explained through the seasonal evolution in the phytoplankton community and the food web structure (e.g., Simó and Pedrós-Alió 1999a; Simó et al. 2002). The seasonal evolution in phytoplankton community composition in the deep chlorophyll maximum layer at BATS has a characteristic pattern of spring bloom conditions followed by a diverse community with increased contributions from prymnesiophytes in the spring and early summer, prochlorophytes and cyanobacteria in late spring to early fall, and pelagophytes increasing in late summer (e.g., Steinberg et al. 2001). Dinoflagellates and prasinophytes make a small contribution annually. At this depth horizon, the phytoplankton community structure does shift to species associated with higher DMSP production, but this production is not evident in the time series of DMSP stocks (Fig. 1B). In addition, in highly oligotrophic regions, the food web is dominated by recycling organisms, providing more opportunity for processing of DMSP.

Ultimately, the importance of DMS photolysis as a loss mechanism is gauged by comparing the photolysis-specific turnover rates to the specific turnover rates of sea–air flux and bacterial consumption. There have been startlingly few studies in open ocean regions that have attempted to concurrently sample all relevant parameters to make this assessment. At our study site, using standard flux parameterizations (Liss and Merlivat 1986) and concurrently measured wind speed, sea–air flux-specific turnover rates in the surface mixed layer range from  $\sim 0$ – $0.18 \text{ d}^{-1}$  (mean =  $0.03 \text{ d}^{-1}$ ) in the winter to  $\sim 0$ – $0.31 \text{ d}^{-1}$  (mean =  $0.04 \text{ d}^{-1}$ ) in the summer. Although there are days where sea–air losses can be quite high because of isolated wind events, the low mean specific turnover rates indicate that, seasonally, photolysis is a larger DMS sink.

Bacterial consumption rates typically show a high degree of variability in open ocean sites (e.g., Kiene and Bates 1990; Kieber et al. 1996; Ledyard and Dacey 1996; Wolfe et al. 1999). Ledyard and Dacey (1996) found net bacterial consumption rates in the surface mixed layer that ranged from  $0.02$  to  $0.15 \text{ nmol L}^{-1} \text{ h}^{-1}$  for this site during the winter and were negligible in the summer. These bacterial consumption rates can be applied to the Dacey et al. (1998) depth-integrated DMS concentrations to yield estimated bacterial specific turnover rates. The consumption rates were assumed constant throughout the mixed layer, yielding turnover rates ranging from  $0.09$ – $1.4 \text{ d}^{-1}$  (assuming  $0.02 \text{ nmol L}^{-1} \text{ h}^{-1}$ ) to  $>5 \text{ d}^{-1}$  (assuming  $0.15 \text{ nmol L}^{-1} \text{ h}^{-1}$ ) in the winter. These are likely to be maximal rates, however, because Ledyard and Dacey's (1996) incubations were conducted in amber Qorpak bottles, which do not allow for photoinhibition. In addition, the fact that they observed no ap-

preciable net bacterial consumption in the summer, along with the previously mentioned bacterial consumption inhibition, suggests significantly longer biological turnover times during time periods of high UV flux.

In absolute terms, because we did not concurrently measure bacterial consumption, we cannot assess the relative importance of photolysis to total DMS loss during the study period. A recent study indicates that under typical surface irradiation conditions, DMS photolysis is always more rapid than bacterial consumption (Slezak et al. 2001). In a short-term Lagrangian study in the subpolar North Atlantic, Simó et al. (1999b) estimated all loss pathways in the mixed layer and demonstrated that for the first 5 d, characterized by clear skies, photolysis was the dominant DMS sink, whereas for the remaining 9 d, characterized by lower solar radiation because of clouds, bacterial consumption dominated. Although the importance of these two loss terms will vary as a function of irradiance, water clarity, temperature, and bacterial activity and sulfur demands, there are clearly time periods and depth regions where each process will dominate.

It is clear from this study that DMS photolysis significantly limits the buildup of upper ocean DMS but does not drive the summer paradox in the Sargasso Sea. Moreover, light has a complex and variable role in the biogeochemical cycling of sulfur on adaptations and inhibition of individual species and communities. DMS and DMSP contribute a large portion of the organic sulfur fluxes and a significant portion of the total carbon flux through primary and secondary producers (e.g., Kiene et al. 2000; Burkill et al. 2002; Simó et al. 2002). Knowledge of these food web interactions is critical for developing a predictive understanding of DMS cycling and its exchange with the atmosphere. The potential radiative and climatic ramifications resulting from a decoupling of production and loss of DMS further necessitate understanding the spatial and temporal variations in the relevant mechanisms that control DMS concentrations in the upper water column. Without a more complete understanding of the complex and dynamic food web interactions and a way to independently measure production and removal terms, it is difficult to determine the origins of the summer paradox.

## References

- ANDREAE, M. O. 1986. The ocean as a source of atmospheric sulfur compounds, p. 331–362. *In* P. Buat-Menard [ed.], *The role of air–sea exchange in geochemical cycling*. Academic.
- BATES, T. S., R. J. CHARLSON, AND R. H. GAMMON. 1987. Evidence for the climatic role of marine biogenic sulphur. *Nature* **329**: 319–321.
- BRIMBLECOMBE, P., AND D. SHOOTER. 1986. Photo-oxidation of dimethylsulphide in aqueous solution. *Mar. Chem.* **19**: 343–353.
- BRUGGER, A., D. SLEZAK, I. OBERNOSTERER, AND G. J. HERNDL. 1998. Photolysis of dimethylsulfide in the northern Adriatic Sea: Dependence on substrate concentration, irradiance and DOC concentration. *Mar. Chem.* **59**: 321–331.
- BURKILL, P. H., S. D. ARCHER, C. ROBINSON, P. D. NIGHTINGALE, S. B. GROOM, G. A. TARRAN, AND M. V. ZUBKOV. 2002. Dimethyl sulphide biogeochemistry within a coccolithophore bloom (DISCO): An overview. *Deep-Sea Res.* **49**: 2863–2885.
- CHARLSON, R. J., J. E. LOVELOCK, M. O. ANDREAE, AND S. G. WARREN. 1987. Oceanic phytoplankton, atmospheric sulfur, cloud albedo and climate. *Nature* **326**: 655–661.
- DACEY, J. W. H., AND S. G. WAKEHAM. 1986. Oceanic dimethylsulfide: Production during zooplankton grazing on phytoplankton. *Science* **233**: 1314–1316.
- , F. A. HOWSE, A. F. MICHAELS, AND S. G. WAKEHAM. 1998. Temporal variability of dimethylsulfide and dimethylsulfoniopropionate in the Sargasso Sea. *Deep-Sea Res.* **45**: 2085–2104.
- GORDON, H. R., AND A. MOREL. 1983. Remote assessment of ocean color for interpretation of satellite visible imagery, a review; lecture notes on coastal and estuarine studies, v. 4. Springer-Verlag.
- GREEN, S. A., AND N. V. BLOUGH. 1994. Optical absorption and fluorescence properties of chromophoric dissolved organic matter in natural water. *Limnol. Oceanogr.* **39**: 1903–1916.
- HATTON, A. D. 2002. Influence of photochemistry on the marine biogeochemical cycle of dimethylsulphide in the northern North Sea. *Deep-Sea Res.* **49**: 3039–3052.
- HERNDL, G. J., G. MULLER-NIKLAS, AND J. FRICK. 1993. Major role of ultraviolet-B in controlling bacterioplankton growth in the surface layer of the ocean. *Nature* **361**: 717–719.
- JANKOWSKI, J. J., D. J. KIEBER, AND K. MOPPER. 1999. Nitrate and nitrite ultraviolet actinometers. *Photochem. Photobiol.* **70**: 319–328.
- , ———, ———, AND P. J. NEALE. 2000. Development and intercalibration of ultraviolet solar actinometers. *Photochem. Photobiol.* **71**: 431–440.
- JODWALIS, C. M., R. L. BENNER, AND D. L. ESLINGER. 2000. Modeling of dimethyl sulfide ocean mixing, biological production, and sea-to-air flux for high latitudes. *J. Geophys. Res.* **105**: 14,387–14,399.
- KELLER, M. D., W. K. BELLOWS, AND R. R. L. GUILLARD. 1989. Dimethyl sulfide production in marine phytoplankton, p. 167–182. *In* E. Saltzman and W. J. Cooper [eds.], *Biogenic Sulfur in the Environment*. American Chemical Society Symposium Series No. 393. Am. Chem. Soc., Washington, D.C.
- KIEBER, D. J. 2000. Photochemical production of biological substrates, p. 130–148. *In* S. J. de Mora, S. Demers, and M. Vernet [eds.], *The effects of UV radiation in the marine environment*. Cambridge.
- , J. JIAO, R. P. KIENE, AND T. S. BATES. 1996. Impact of dimethylsulfide photochemistry on methyl sulfur cycling in the equatorial Pacific Ocean. *J. Geophys. Res.* **101**: 3715–3722.
- , B. H. YOCIS, AND K. MOPPER. 1997. Free-floating drifter for photochemical studies in the water column. *Limnol. Oceanogr.* **42**: 1829–1833.
- KIENE, R. P., AND T. S. BATES. 1990. Biological removal of dimethylsulfide from sea water. *Nature* **345**: 702–705.
- , AND S. K. SERVICE. 1991. Decomposition of dissolved DMSO and DMS in estuarine waters: Dependence on temperature and substrate concentration. *Mar. Ecol. Prog. Ser.* **76**: 1–11.
- , L. J. LINN, J. GONZALEZ, M. A. MORAN, AND J. A. BRUTON. 1999. Dimethylsulfoniopropionate and methanethiol are important precursors of methionine and protein-sulfur in marine bacterioplankton. *Appl. Environ. Microbiol.* **65**: 4549–4558.
- , ———, AND J. A. BRUTON. 2000. New and important roles for DMSP in marine microbial communities. *J. Sea Res.* **43**: 209–224.
- KIRK, J. T. O. 1981. Estimation of the scattering coefficient of natural waters using underwater irradiance measurements. *Aust. J. Mar. Freshw. Res.* **32**: 333–339.
- LEDYARD, K. M., AND J. W. H. DACEY. 1996. Microbial cycling of DMSP and DMS in coastal and oligotrophic seawater. *Limnol. Oceanogr.* **41**: 33–40.

- LISS, P. S., AND L. MERLIVAT. 1986. Air-sea gas exchange rates: Introduction and synthesis, p. 113–127. *In* P. Buat-Menard [ed.], *The role of air-sea exchange in geochemical cycling*. Academic.
- LUBIN, D., E. H. JENSEN, AND H. P. GIES. 1998. Global surface ultraviolet radiation climatology from TOMS and ERBE data. *J. Geophys. Res.* **103**: 26,061–26,091.
- MARITORENA, S., D. A. SIEGEL, AND A. R. PETERSON. 2002. Optimization of a semi-analytical ocean color model for global-scale applications. *Appl. Opt.* **41**: 2705–2714.
- MILLER, G. W. 2000. Wavelength and temperature dependent quantum yields for photochemical formation of hydrogen peroxide in seawater. M.S. thesis, State Univ. of New York, College of Environmental Science and Forestry.
- MOBLEY, C. D. 1994. Light and water, radiative transfer in natural waters. Academic.
- NEALE, P. J., AND D. J. KIEBER. 2000. Assessing biological and chemical effects of UV in the marine environment: Spectral weighting functions, p. 61–83. *In* R. E. Hester and R. M. Harrison [eds.], *Causes and environmental implications of increased UV-B radiation*. The Royal Society of Chemistry.
- NELSON, N. B., AND D. A. SIEGEL. 2002. Chromophoric DOM in the open ocean, p. 547–578. *In* D. A. Hansell and C. A. Carlson [eds.], *Biogeochemistry of marine dissolved organic matter*. Academic.
- , ———, AND A. F. MICHAELS. 1998. Seasonal dynamics of colored dissolved material in the Sargasso Sea. *Deep-Sea Res.* **45**: 931–957.
- POPE, R. M., AND E. S. FRY. 1997. Absorption spectrum (380–700 nm) of pure water. 2. Integrating cavity measurements. *Appl. Opt.* **36**: 8710–8723.
- SHAW, G. E. 1983. Bio-controlled homeostasis involving the sulfur cycle. *Climate Chang.* **5**: 297–303.
- SHOOTER, D., AND P. BRIMBLECOMBE. 1989. Dimethylsulphide oxidation in the ocean. *Deep-Sea Res.* **36**: 577–585.
- SIEGEL, D. A., AND A. F. MICHAELS. 1996. Quantification of non-algal light attenuation in the Sargasso Sea: Implications for biogeochemistry and remote sensing. *Deep-Sea Res.* **43**: 321–345.
- , AND OTHERS. 2001. Bio-optical modeling of primary production on regional scales: The Bermuda BioOptics project. *Deep-Sea Res.* **48**: 1865–1896.
- , S. MARITORENA, N. B. NELSON, D. A. HANSELL, AND M. LORENZI-KAYSER. 2002. Global distribution and dynamics of colored dissolved and detrital organic materials. *J. Geophys. Res.* **107**, 3228, doi:10.1029/2001JC000965.
- SIMÓ, R., AND C. PEDRÓS-ALIÓ. 1999a. Role of vertical mixing in controlling the oceanic production of dimethyl sulphide. *Nature* **402**: 396–399.
- , AND ———. 1999b. Short-term variability in the open ocean cycle of dimethylsulphide. *Glob. Biogeochem. Cycles* **13**: 1173–1181.
- , S. D. ARCHER, C. PEDRÓS-ALIÓ, L. GILPIN, AND C. E. STELFOX-WIDDICOMBE. 2002. Coupled dynamics of dimethylsulfoniopropionate and dimethylsulfide cycling and the microbial food web in surface waters of the North Atlantic. *Limnol. Oceanogr.* **47**: 53–61.
- SLEZAK, D., A. BRUGGER, AND G. J. HERNDL. 2001. Impact of solar radiation on the biological removal of dimethylsulfoniopropionate and dimethylsulfide in marine surface waters. *Aquat. Microb. Ecol.* **25**: 87–97.
- STEINBERG, D. K., C. A. CARLSON, N. R. BATES, R. J. JOHNSON, A. F. MICHAELS, AND A. H. KNAP. 2001. Overview of the US JGOFS Bermuda Atlantic Time-series Study (BATS): A decade-scale look at ocean biology and biogeochemistry. *Deep-Sea Res.* **48**: 1405–1447.
- SUNDA, W., D. J. KIEBER, R. P. KIENE, AND S. HUNTSMAN. 2002. An antioxidant function for DMSP and DMS in marine algae. *Nature* **418**: 317–320.
- VAN DEN BERG, A. J., S. M. TURNER, F. C. VAN DUYL, AND P. RUARDIJ. 1996. Model structure and analysis of dimethylsulfide (DMS) production in the southern North Sea, considering phytoplankton dimethylsulphoniopropionate (DMSP) lyase and eutrophication effects. *Mar. Ecol. Prog. Ser.* **145**: 233–244.
- WEISS, P. S., S. S. ANDREWS, J. E. JOHNSON, AND O. C. ZAFIRIOU. 1995. Photoproduction of carbonyl sulfide in south Pacific Ocean waters as a function of irradiation wavelength. *Geophys. Res. Lett.* **22**: 215–218.
- WOLFE, G. V., M. LEVASSEUR, G. CANTIN, AND S. MICHAUD. 1999. Microbial consumption and production of dimethyl sulfide (DMS) in the Labrador Sea. *Aquat. Microb. Ecol.* **18**: 197–205.
- XIE, H., R. M. MOORE, AND W. L. MILLER. 1998. Photochemical production of carbon disulphide in seawater. *J. Geophys. Res.* **103**: 5635–5644.
- YOCIS, B. H., D. J. KIEBER, AND K. MOPPER. 2000. Photochemical production of hydrogen peroxide in Antarctic waters. *Deep-Sea Res.* **47**: 1077–1099.

*Received: 12 August 2002*  
*Accepted: 19 January 2003*  
*Amended: 5 February 2003*